

We are IntechOpen, the world's leading publisher of Open Access books Built by scientists, for scientists

4,800

Open access books available

122,000

International authors and editors

135M

Downloads

Our authors are among the

154

Countries delivered to

TOP 1%

most cited scientists

12.2%

Contributors from top 500 universities



WEB OF SCIENCE™

Selection of our books indexed in the Book Citation Index
in Web of Science™ Core Collection (BKCI)

Interested in publishing with us?
Contact book.department@intechopen.com

Numbers displayed above are based on latest data collected.
For more information visit www.intechopen.com



Beach Changes on Coast Subject to Waves and Seaward or Shoreward Strong Currents

Takaaki Uda, Masumi Serizawa and Shiho Miyahara

Abstract

Beach changes on a coast subject to waves and seaward or shoreward strong currents were predicted using the Type 7 and 8 BG models. The formation of an ebb tidal delta subject to strong ebb tidal currents was studied first, taking the Imagire-guchi inlet connecting Lake Hamana with the Pacific Ocean as an example, and the long-term evolution of the tidal inlet was investigated using the bathymetric survey data. Then, the formation of a dynamically stable ebb tidal delta was predicted. Regarding the beach changes on a coast subject to waves and shoreward strong currents, the Type 8 was applied to the Kaike coast, where an artificial reef was constructed in place of a detached breakwater, resulting in the occurrence of strong shoreward currents over the artificial reef. A stable cusped foreland behind a detached breakwater disappeared after the conversion of a detached breakwater into an artificial reef, suggesting that the artificial reef was less effective in sand deposition effect than the detached breakwater. Such beach changes were numerically predicted.

Keywords: ebb tidal delta, Lake Hamana, Imagire-guchi inlet, artificial reef, Kaike coast

1. Introduction

In predicting beach changes on a coast subject to not only waves but also seaward or shoreward strong currents, the effect of both waves and strong currents must be taken into account. As the beach changes on a coast subject to waves and seaward strong currents, the formation of an ebb tidal delta under strong ebb tidal currents at an inlet was considered, taking the Imagire-guchi inlet connecting Lake Hamana with the Pacific Ocean, as an example, and the long-term evolution of the tidal inlet was studied using the bathymetric survey data. The past studies have revealed that the jetty at this inlet blocks predominant westward longshore sand transport, causing downcoast erosion. However, not only shoreline changes but also complicated, large-scale 3-D beach changes have occurred around this tidal inlet due to the strong ebb tidal currents along with the action of rough waves from the Pacific Ocean. Sand supplied from upcoast has flowed out to the offshore zone, forming a large ebb tidal delta. In the comprehensive management of the coast, the loss of sand into the offshore zone is of importance, but the quantitative prediction of the bathymetric changes around this tidal inlet was difficult in the past because of the combined action of waves and tidal currents. In Section 2, bathymetric changes between 1978 and 2005 around this inlet, for which the characteristics of tidal currents have been

measured by Syamsidik et al. [1], were investigated, and the evolution of an ebb tidal delta and bathymetric changes were predicted using the Type 7 BG model [2, 3].

It is well known that strong shoreward currents are induced by the wave breaking on the artificial reef, i.e., a kind of submerged breakwater, resulting in significant beach changes around the artificial reef. In Section 3, the Kaike coast was adopted as an example, where an artificial reef was reconstructed in place of a detached breakwater and then strong shoreward currents were induced over the artificial reef, causing significant beach changes around the artificial reef. The beach changes associated with the conversion from the detached breakwater to an artificial reef on this coast were measured, and the Type 8 BG model was used to predict beach changes [4]. It was concluded that a stable cusped foreland behind a detached breakwater disappeared after the conversion of a detached breakwater into an artificial reef, implying that the artificial reef was less effective in sand deposition effect than the detached breakwater.

2. Prediction of formation of dynamically stable ebb tidal delta

2.1 General condition of Imagire-guchi jetty

A jetty had been built at the Imagire-guchi inlet to stabilize the tidal inlet and to enhance the safety of the navigation of fishing boats in Maisaka fishing port located inside the lake, as shown in **Figure 1** [2].

This jetty blocked predominant westward longshore sand transport, causing accretion upcoast and downcoast erosion, and a part of sand supplied from the upcoast has transported offshore by ebb tidal currents, forming a large ebb tidal delta and causing loss of a part of foreshore sand. The bathymetric changes associated with the extension of Imagire-guchi jetty were studied based on the bathymetric survey data in the previous work [2]. The channel connecting Lake Hamana with the Pacific Ocean and the parallel jetty shown in **Figure 1** had already been built by 1964. By 1973, an oblique jetty of 200 m length had been extended at the tip of the east jetty; this oblique jetty forced the direction of ebb tidal currents clockwise, and this accelerated the southwestward development of the foreset slope together with the blockage of westward

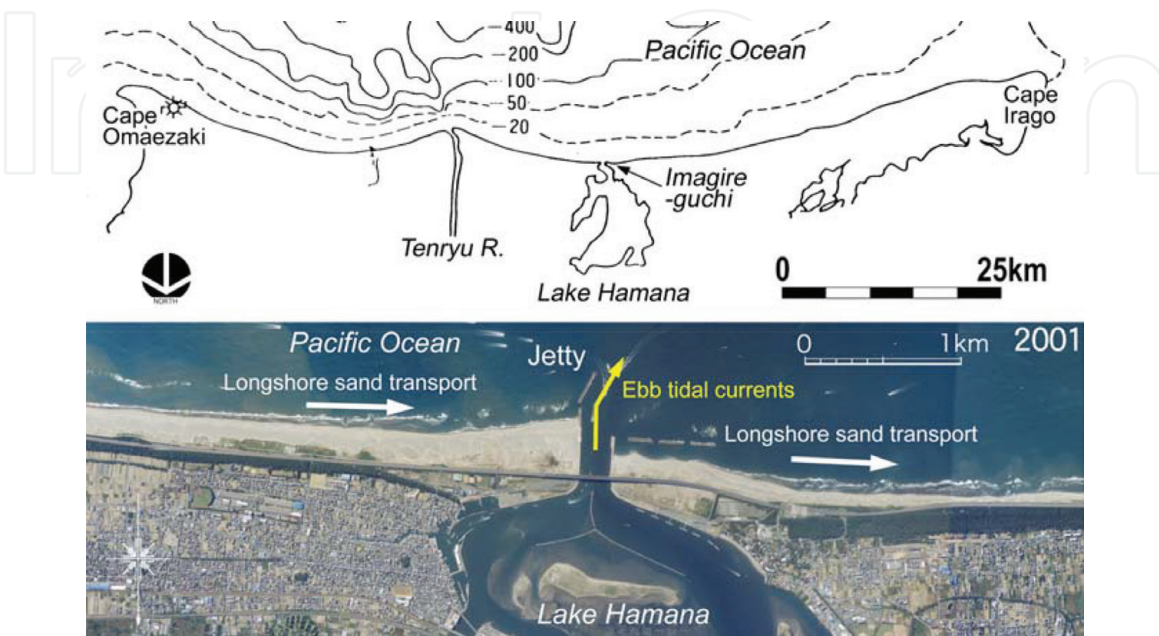


Figure 1.
Location of Imagire-guchi inlet on Enshu-nada coast.

longshore sand transport [2]. Furthermore, two detached breakwaters had been built by 1990 and another by 1994 west of the inlet. Finally, the present shoreline, as shown in **Figure 1**, was formed around the Imagire-guchi inlet.

2.2 Calculation conditions

The evolution of ebb tidal delta offshore of Imagire-guchi jetty was predicted using the Type 7 BG model. To this purpose, the coastal domain was discretized in 2-D elements with dimensions Δx and Δy . Given the initial topography, H_b , α_b , h_c , h_R , the equilibrium slope, and various conditions of the ebb tidal currents, sand transport fluxes due to waves and the ebb tidal currents were calculated from Eqs. (43) and (45) in Chapter 2, respectively. Finally, the sum of them was obtained from Eq. (42) in Chapter 2, and the beach changes after Δt were calculated from the continuity equation of the sand. These calculations were repeated.

For the boundary conditions, sand transport across the boundary was set to be 0 at the structural boundary. **Figure 2** shows the initial bathymetry. Although both actions of waves and ebb tidal currents simultaneously occur at the tidal inlet, it was assumed that sand supply during the ebb tidal currents was none. In the calculation, the change in wave energy intensity associated with the wave refraction was neglected for simplicity, and we assumed that $\cos\alpha_b = 1$. In addition, the lower-limit depth of bathymetric changes due to tidal currents h_{c2} was assumed to be equal to the depth of closure due to waves, h_c , and the upper-limit depth of bathymetric changes due to tidal currents h_{R2} was taken at the mean sea level. In the calculation of Eq. (48) in Chapter 2, a minimum value of $h_0 = 1$ m was assumed for h .

The distribution of the ebb tidal currents through a tidal inlet is very similar to that of a jet flowing into a still water, which in turn is similar to the distribution of the wave diffraction coefficient of the diffracted waves through the opening of the impermeable breakwaters [2]. Taking this fact into account, the angular spreading method for irregular waves [5] was introduced to calculate the ratio of the velocity K_{V1} , as shown in Eq. (49) in Chapter 2, under a constant depth condition. Assume that the directional spreading of a jetlike flow at the tidal inlet is given by the directional spreading function of wave energy $G(\theta)$ in the angular spreading method and that the ratio of the wave energy, which is given by the square of the wave diffraction coefficient, is equal to the velocity ratio. Then, the reduction of the velocity of a jetlike flow can be evaluated while satisfying the mass conservation condition.

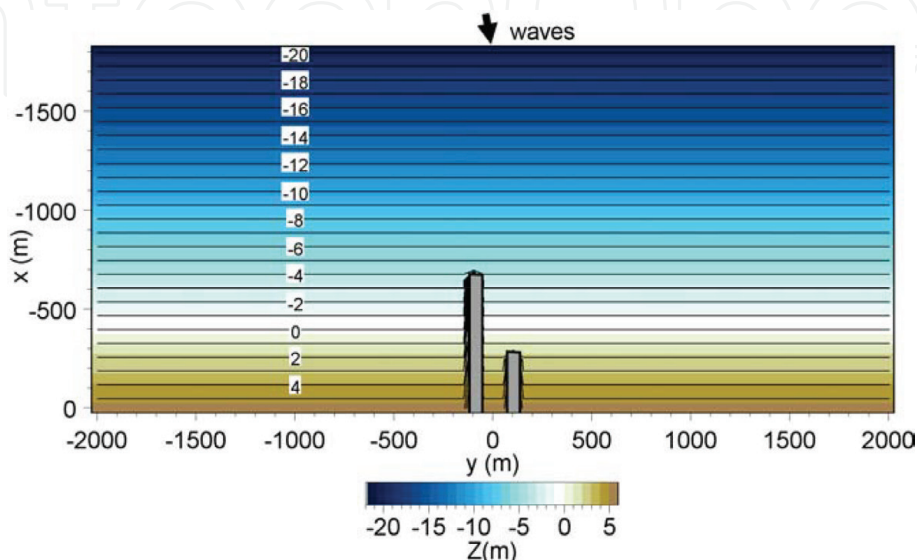


Figure 2.
 Initial bathymetry.

When setting the range of the flow direction with respect to the center line of the jetlike flow as $\theta = -\theta_{\max} \sim \theta_{\max}$, θ_{\max} becomes $\pi/2$ for the irregular waves, but the range becomes as narrow as $\theta_{\max} = 11^\circ$ for a jetlike flow. Furthermore, the diffusivity of a jetlike flow can be evaluated by a parameter A_0 in the angular spreading method [5] expressing the directional distribution function of the wave energy. Finally, regarding the tidal inlet as an opening of the impermeable breakwaters, irregular waves propagating offshore were generated, and the wave diffraction coefficient was calculated using the angular spreading method. The ratio of the wave energy and wave direction of diffracted waves was substituted for the ratio of flow velocity and the direction of the flow, respectively, assuming that θ_{\max} and A_0 are 15° and 5, respectively.

In this study, bathymetric survey data collected since 1978 were used to validate the numerical model, and the sand movement around the ebb tidal delta and the formation of dynamically stable topography were investigated. Given the parallel contours before the construction of the jetty as the initial condition, the bathymetry in 1978 was first predicted, and then the bathymetric changes since 1978 were predicted, enabling the comparison of the predicted development of the ebb tidal delta with measurements. During this period, the ebb tidal currents were intensified because of the scouring at the inlet associated with the extension of the jetty. The coefficient of intensity of sand transport due to ebb tidal currents, therefore, was linearly increased over time from $K_R = 0.1$ in 1978 to 0.3 in 2005 in the calculation.

The east jetty at Imagire-guchi is longer than the west jetty, causing the development of oblique ebb tidal currents. The effect of oblique currents between jetties of different lengths was modeled by a jet obliquely emerging from the inlet at an angle of 30° relative to the direction normal to the shoreline, so that the assumed direction of the jet currents coincides with that of the ebb tidal currents measured at Imagire-guchi inlet by Syamsidik et al. [1]. **Figure 3** shows the velocity distribution when ebb tidal currents obliquely flow out of the inlet.

The calculation conditions are summarized in **Table 1**. Assuming that the breaker height H_b was 3 m and the incident angle of waves at the breaking point was $\alpha_b = 10^\circ$, the coefficient of longshore sand transport K_y was adjusted so that the initial longshore sand transport was $2.0 \times 10^5 \text{ m}^3/\text{year}$, by which the best fit results for the beach changes were obtained, and the dynamically stable condition was reproduced by setting $K_x = 0.2K_y$, where K_x is the coefficient of cross-shore sand transport. The calculation results were presented in a coordinate system (X, Y) , in which the X - and Y -axes were taken to be the longshore and cross-shore directions (positive for offshore), respectively.

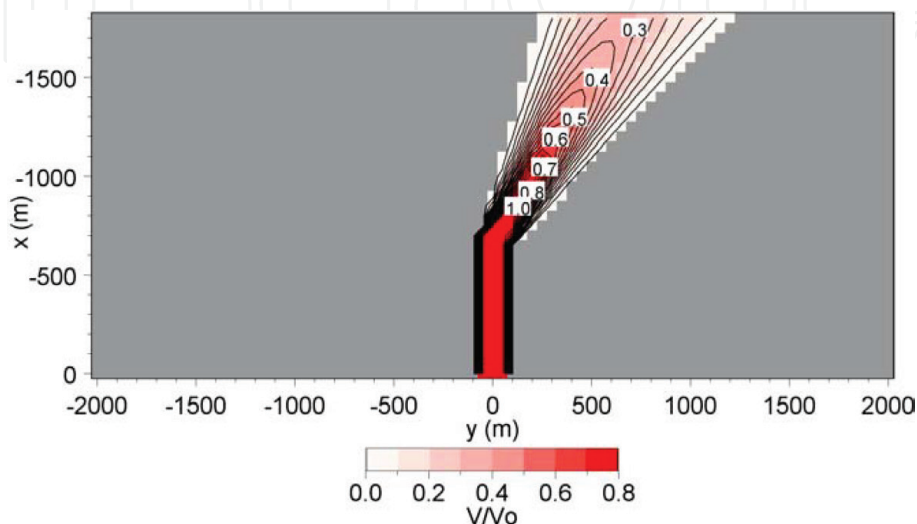


Figure 3.
Example of velocity distribution.

Calculation method	Type 7 BG model
Initial topography	Uniform slope of 1/70
Equilibrium slope	$\tan\beta_c = 1/70$
Slope of angle of repose	$\tan\phi = 1/2$
Wave conditions	$H_b = 3$ m, breaker angle $\theta_w = 10^\circ$, $H_{b0} = 1$ m in calculating $(EC_g)_{b0}$
Depth distribution of intensity of longshore sand transport	Uniform
Coefficients of longshore and cross-shore sand transport	$K_y = 0.0105$ and $K_x = 0.2K_y$
Berm height	$h_R = 3$ m
Depth of closure	$h_c = 8$ m
Coefficient of sediment transport due to ebb tidal currents	$K_R = 0.1-0.3$ for reproduction and $K_R = 0.3$ for prediction
Upper depth of bathymetric changes induced by tidal currents	$h_{R2} = 0$ m
Lower depth of bathymetric changes induced by tidal currents	$h_{c2} = 8$ m
Reference depth of inlet	$h_0 = 1$ m
Minimum depth for the use of correction term of current velocity	$h = 1$ m
Mesh size	$\Delta x = \Delta y = 50$ m
Time interval	$\Delta t = 5$ hrs
Calculation duration	27 years between 1978 and 2005 in reproduction, 10 years in prediction
Boundary conditions	$q_x = 0$ at landward and offshore boundaries $dq_y/dy = 0$ at side boundaries

Table 1.
 Calculation conditions.

2.3 Calculation results

Figure 4 shows the results of the numerical simulation of the formation of the ebb tidal delta with the sand transport flux, given the initial parallel contours and the velocity distribution (**Figures 2 and 3**), and assuming that waves are obliquely incident from the left. The sand was continuously transported westward (rightward in **Figure 4**) along the outer margin of the ebb tidal delta, forming a dynamically stable beach. Finally, an ebb tidal delta with an oblique principal axis developed offshore of the tidal inlet together with the formation of a steep foreset slope in the zone deeper than 10 m depth. Moreover, a pair of circulating sand transport systems developed on both sides of the principal axis of the jetlike offshore sand transport.

Figure 5 shows the bathymetry measured in 2005 and the change in the 8-m-depth contour over time. It is clear that the ebb tidal delta has developed over time. The predicted and measured bathymetric changes between 1978 and 2005 are shown in **Figure 6**. A sand deposition zone was formed along the margin of the ebb tidal delta, whereas erosion occurred in an extensive area around the tip of the jetty. The predicted and measured topographic changes are in good agreement.

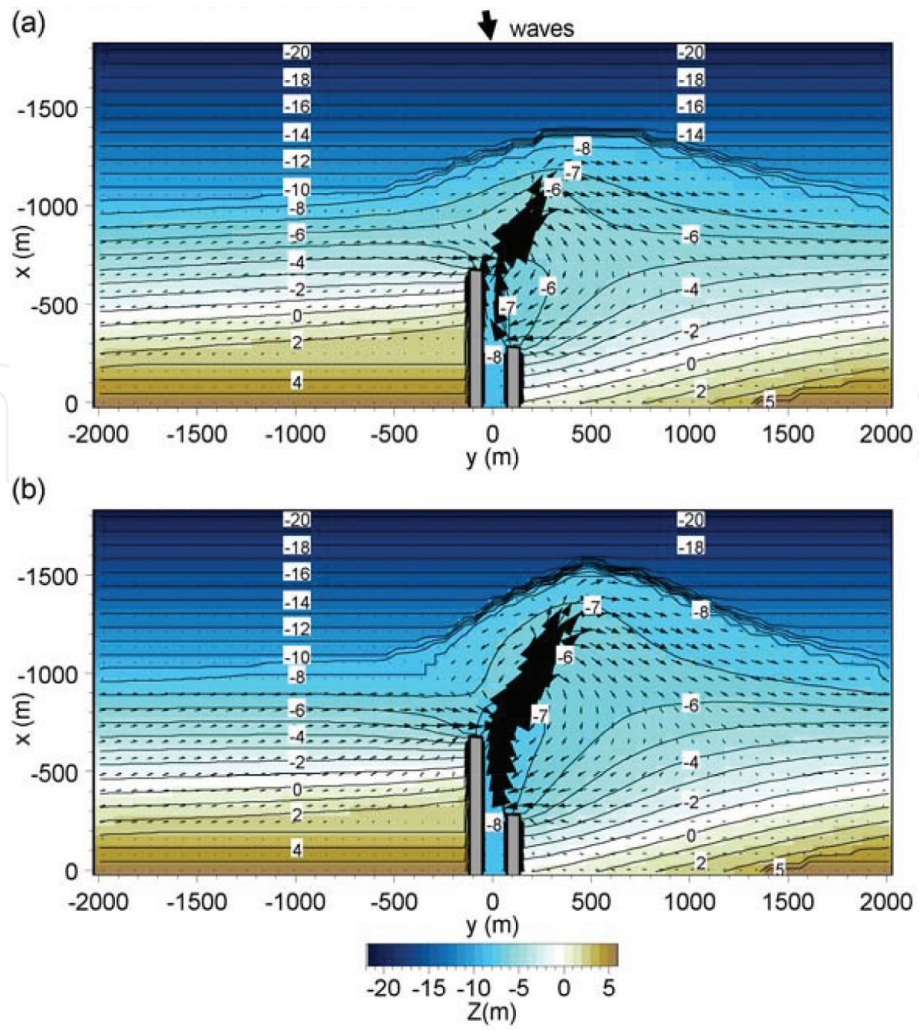


Figure 4. Predicted bathymetries around Imagire-guchi inlet in 1978 and 2005 (a) Predicted bathymetry in 1978, (b) Predicted bathymetry in 2005.

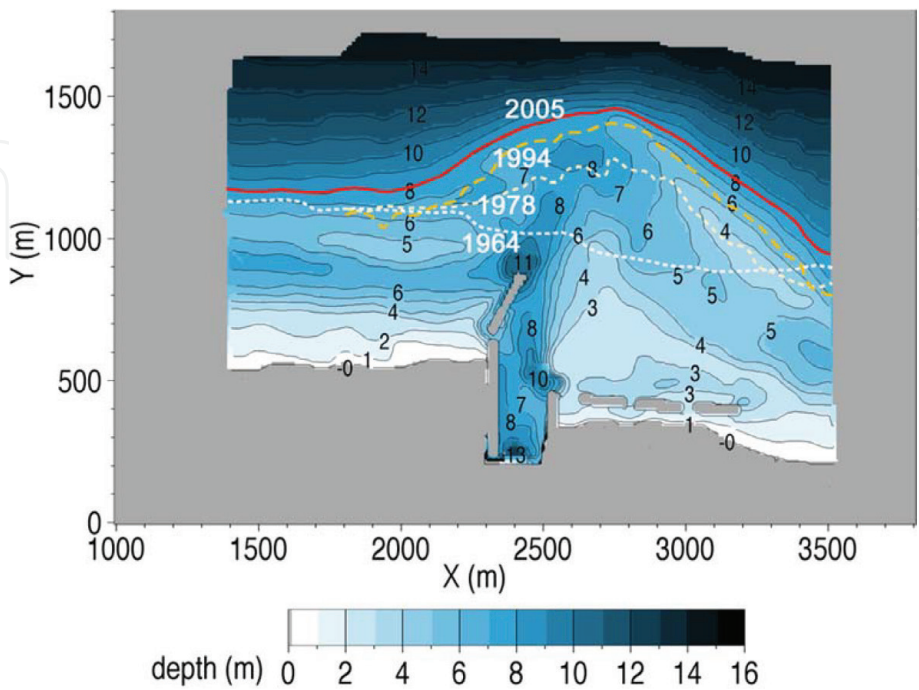


Figure 5. Measured bathymetry in 2005 and change in 8 m contour over time [3].

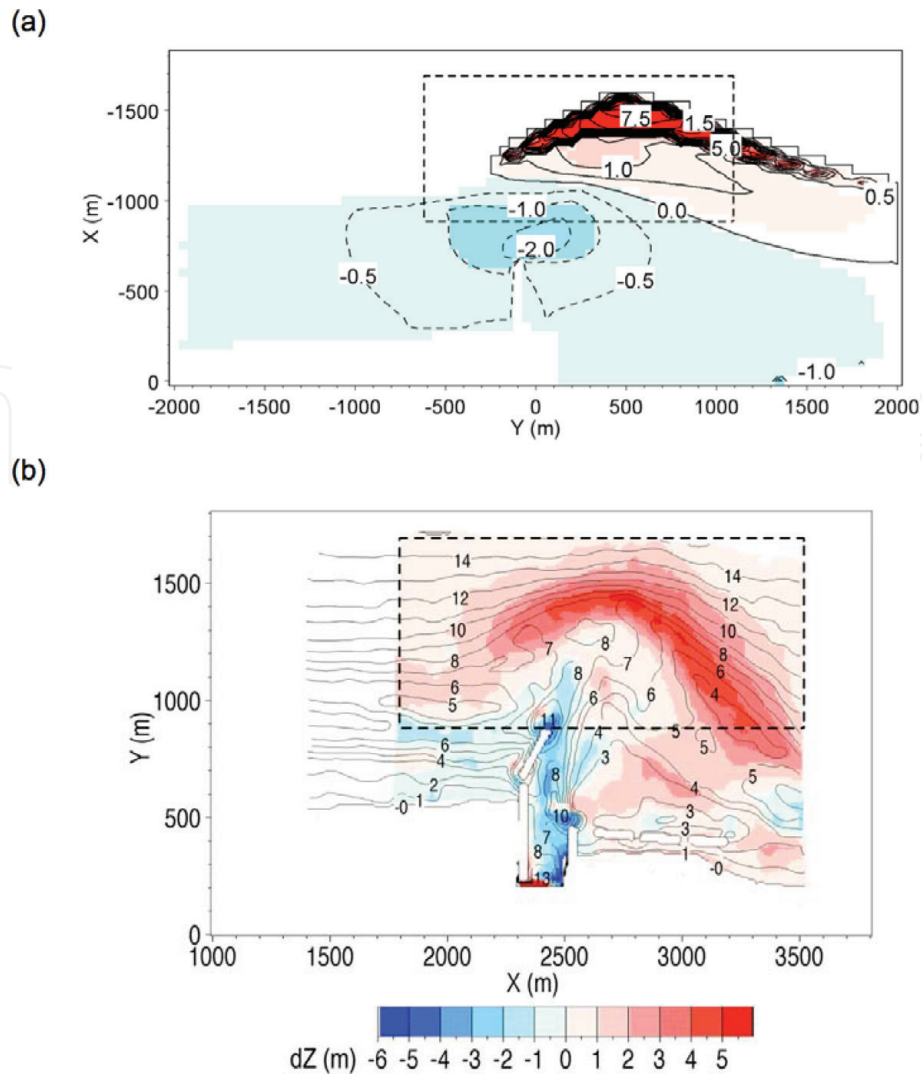


Figure 6.
 Measured and predicted bathymetric changes between 1978 and 2005 [3] (a) predicted, (b) measured.

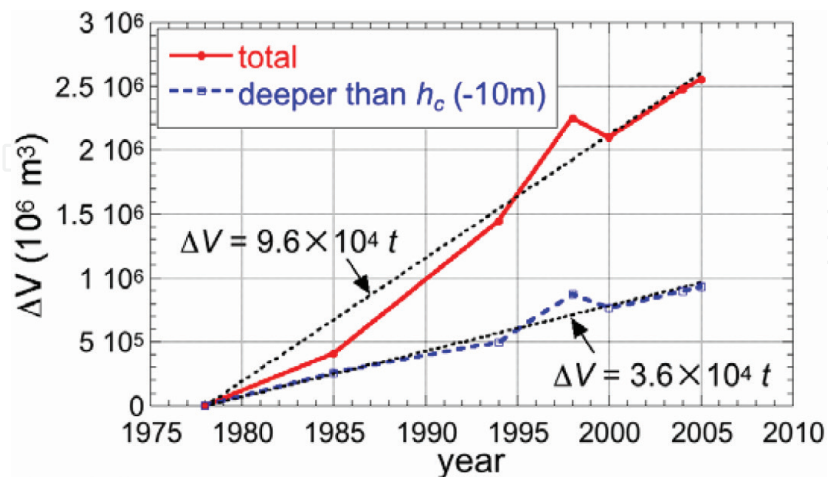


Figure 7.
 Change in sand volume over time in rectangular zone under study [3].

Based on the bathymetric survey data since 1978, the total volume of sand forming the ebb tidal delta and deposited in the zone deeper than h_c of 10 m was calculated. **Figure 7** shows the change in sand volume in a rectangular zone shown by the broken line in **Figure 6**. The total volume of sand increased at a rate of $9.6 \times 10^4 \text{ m}^3/\text{year}$,

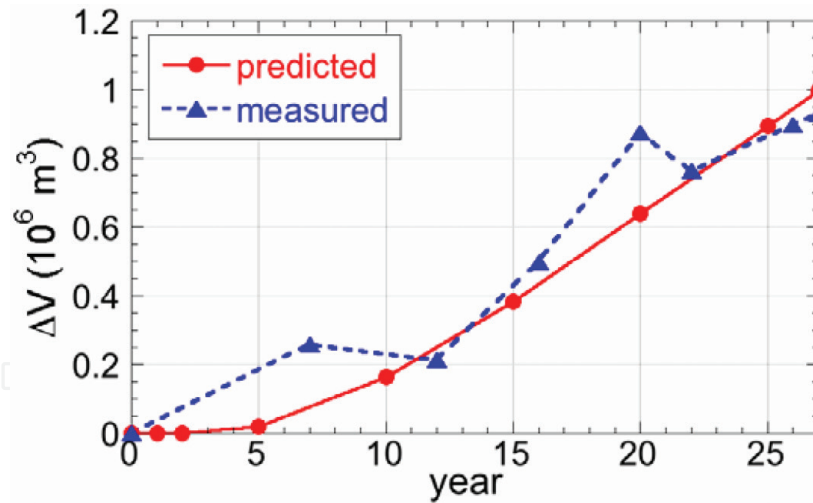


Figure 8. Predicted and measured volumes of sand transported offshore into the zone deeper than 10 m [3].

$3.6 \times 10^4 \text{ m}^3/\text{year}$ of which was transported offshore into the zone deeper than 10 m. The predicted and measured volumes of sand transported offshore into the zone deeper than 10 m can be compared as in **Figure 8**, and both results agree well.

3. Prediction of beach changes around artificial reef built on Kaike coast

3.1 General conditions

The Kaike coast with a 20-km stretch is the marginal coast along the Yumigahama Peninsula in Miho Bay in Tottori Prefecture, Japan, as shown in **Figure 9**. This peninsula has developed as a tombolo by the deposition of sand supplied from the Hino River owing to the wave-sheltering effect of the Shimane Peninsula. After the World War II, beach erosion along the Kaike coast occurred owing to the decrease in sand supply from the Hino River. A famous Kaike spa is located near the shoreline immediately west of the Hino River mouth, and, therefore, the beach around this spa was protected by groynes in the 1960s. Then, 12 detached breakwaters were constructed between 1971 and 1982 as a measure against beach erosion, and soon

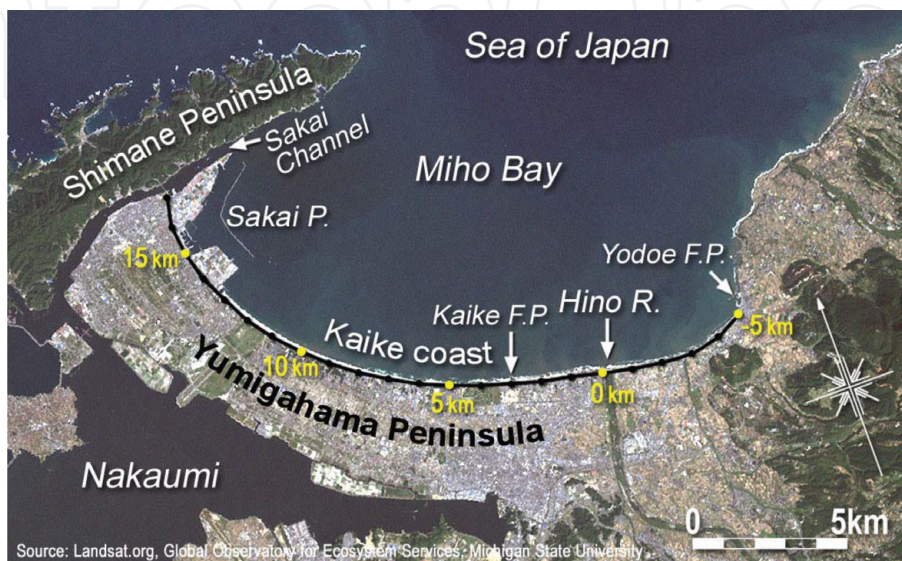


Figure 9. Location of Kaike coast facing the Sea of Japan [4].

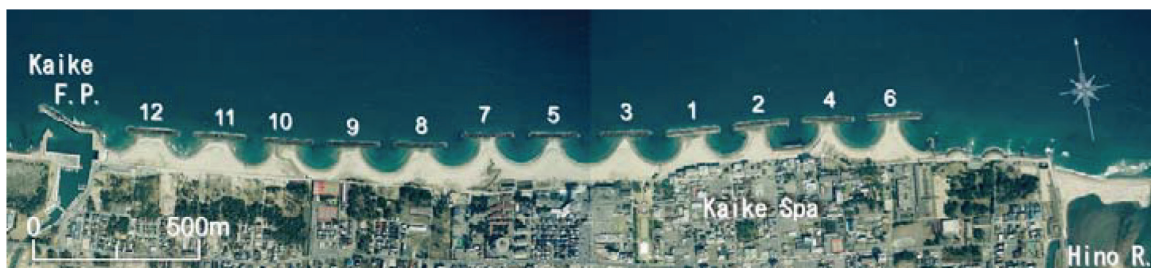


Figure 10.
Aerial photograph of beaches around 12 detached breakwaters on Kaike coast taken in 2003 [4].

after the construction of the detached breakwaters, tombolos were formed behind the detached breakwaters.

Figure 10 shows the aerial photograph in 2003 of the detached breakwaters, in which the number of the breakwaters corresponds to the order of the construction. Although these detached breakwaters and tombolos have been stable until 2003, concrete armor units placed immediately offshore of the shoreline near the spa spoiled the scenic beauty as a recreational beach and extremely narrowed the swimming space, and the foreshore slope was excessively steepened at the opening of the detached breakwaters. Therefore, an artificial reef with crests was constructed in place of the No. 3 detached breakwater in 2005. After the conversion, the tombolo was reduced in size because of the generation of shoreward currents on the artificial reef, and severe scouring occurred at the opening between the artificial reef and the existing detached breakwaters owing to the development of rip currents [4]. Here, the beach changes were predicted using the Type 8 BG model, in which the effect of not only waves but also strong nearshore currents was taken into account, as well as increase in h_c due to the strong currents.

3.2 Beach changes after construction of artificial reef

Figure 11 shows the bathymetry measured in July 2002 before the conversion of the No. 3 detached breakwater into the artificial reef. In 2002, a tombolo was formed behind the Nos. 1, 3, and 5 detached breakwaters owing to their wave-sheltering effect, and semicircular contours were formed at the openings between the detached breakwaters owing to their wave diffraction effects. In addition, the foreshore slope became as steep as 1/7 at the central part of the opening. One of the objectives of converting the detached breakwater into an artificial reef was to create a gentle slope near the shoreline that is considered to be safe for recreational use. The artificial reef had a crown height of 0.5 m below MSL and a width of 40 m, as well as two rows of crests that enhance the wave attenuation effect. Here, HWL and LWL of this coast are +0.36 and - 0.56 m above MSL. After the conversion of the reef, storm waves associated with a low pressure hit the artificial reef in December 2005.

Owing to the wave observation at a depth of 8 m offshore of the artificial reef, storm waves with a maximum significant wave height of 4.5 m and a wave period of 12 s were measured, and storm waves with a wave height of greater than 3 m continued for 30 h. As a result, the tombolo behind the artificial reef was eroded, and the foreshore disappeared (**Figures 12 and 13**). A flat shallow seabed of 2 m depth was formed behind the artificial reef.

Figure 13 shows the bathymetric changes around the artificial reef before and after the construction of the artificial reef. Not only did the tombolo formed behind the detached breakwater disappear, but also a deep scouring hole with a maximum depth of 7 m was formed at the west end of the artificial reef. The local

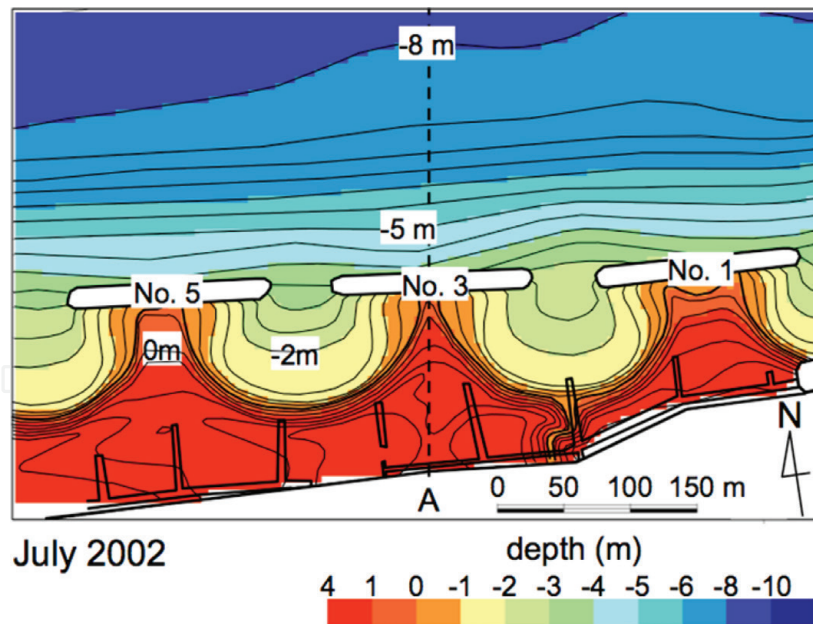


Figure 11.
Bathymetry in July 2002 before conversion of detached breakwater into artificial reef [4].

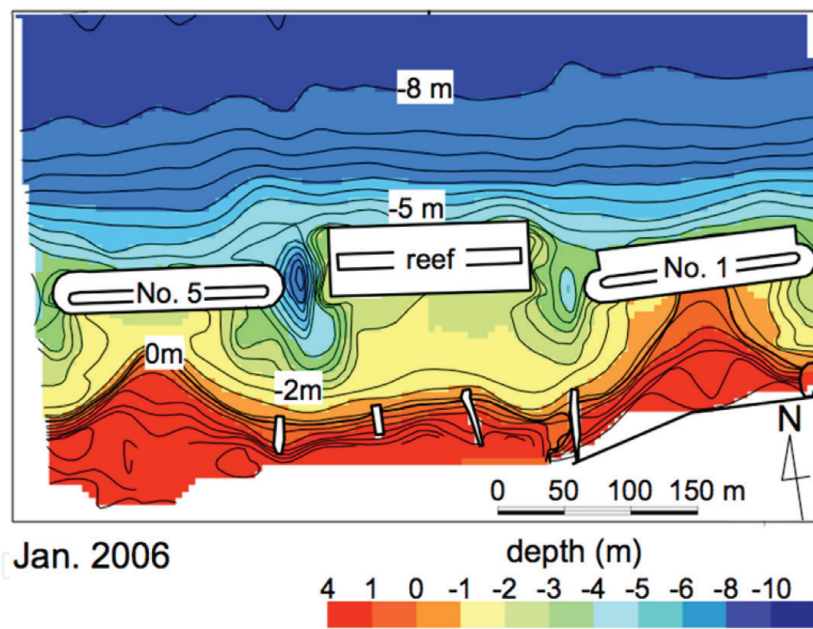


Figure 12.
Bathymetry after storm waves measured in January 2006 [4].

scouring at both ends of the artificial reef showed asymmetry, and the scouring hole at the west opening was larger than that at the east opening. Thus, it is considered that predominant waves were incident from the east, producing westward longshore currents. Furthermore, the tombolo behind the No. 5 detached breakwater west of the artificial reef was eroded and the shoreline retreated, implying the development of westward longshore currents passing through the lee of the No. 5 detached breakwater, which in turn eroded the shoreline on the lee of the No. 5 detached breakwater. Finally, it was found that converting the detached breakwater into an artificial reef caused the disappearance of the tombolo, the local scouring at the opening, and the reduction in the size of the tombolo behind the nearby detached breakwater.

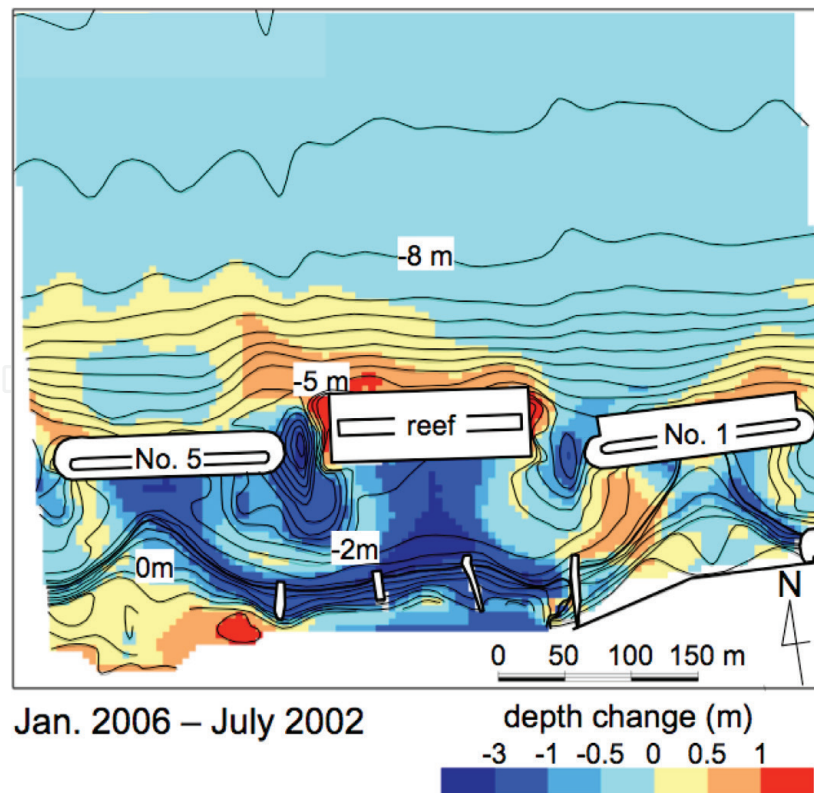


Figure 13.
Bathymetric changes from July 2002 to January 2006 [4].

3.3 Calculation conditions

On the basis of the bathymetric survey data in 2009, a rectangular calculation domain of 1800 m length and 700 m width including the No. 3 detached breakwater, which was later converted into an artificial reef, was adopted. As the initial bathymetry, the condition that tombolos behind the detached breakwaters have sufficiently developed was set (**Figure 14(a)**). The offshore slope was set to be 1/30 in the depth zone between -5 and -8 m and 1/100 deeper than -8 m.

Under these conditions, storm waves with a significant height $H_i = 3$ m and a period of 8 s were obliquely incident from the right at an angle of $\theta_i = 10^\circ$. The wave field and nearshore currents were recalculated at every 5000 steps of the calculation of the topographic changes. **Table 2** summarizes the detailed calculation conditions. h_R was set to be 3 m, and the equilibrium slope was given as in **Table 2**, depending on the water depth, and the slope of the angle of repose was set to be 1/2.

3.4 Calculation results

3.4.1 Beach changes around detached breakwater and artificial reef

Beach changes owing to a 40-h wave action after all the detached breakwaters were installed were calculated, using the bathymetry in **Figure 14(a)** as the initial bathymetry. The predicted bathymetry and the bathymetric changes are shown in **Figures 14(b)** and **14(c)**. In this case, although the beach was slightly eroded around the detached breakwaters and sand was deposited on the foreshore, beach changes were negligibly small, and the cusped forelands behind the detached breakwaters were stable, implying that beach changes around the detached breakwaters could be reproduced by the present model.

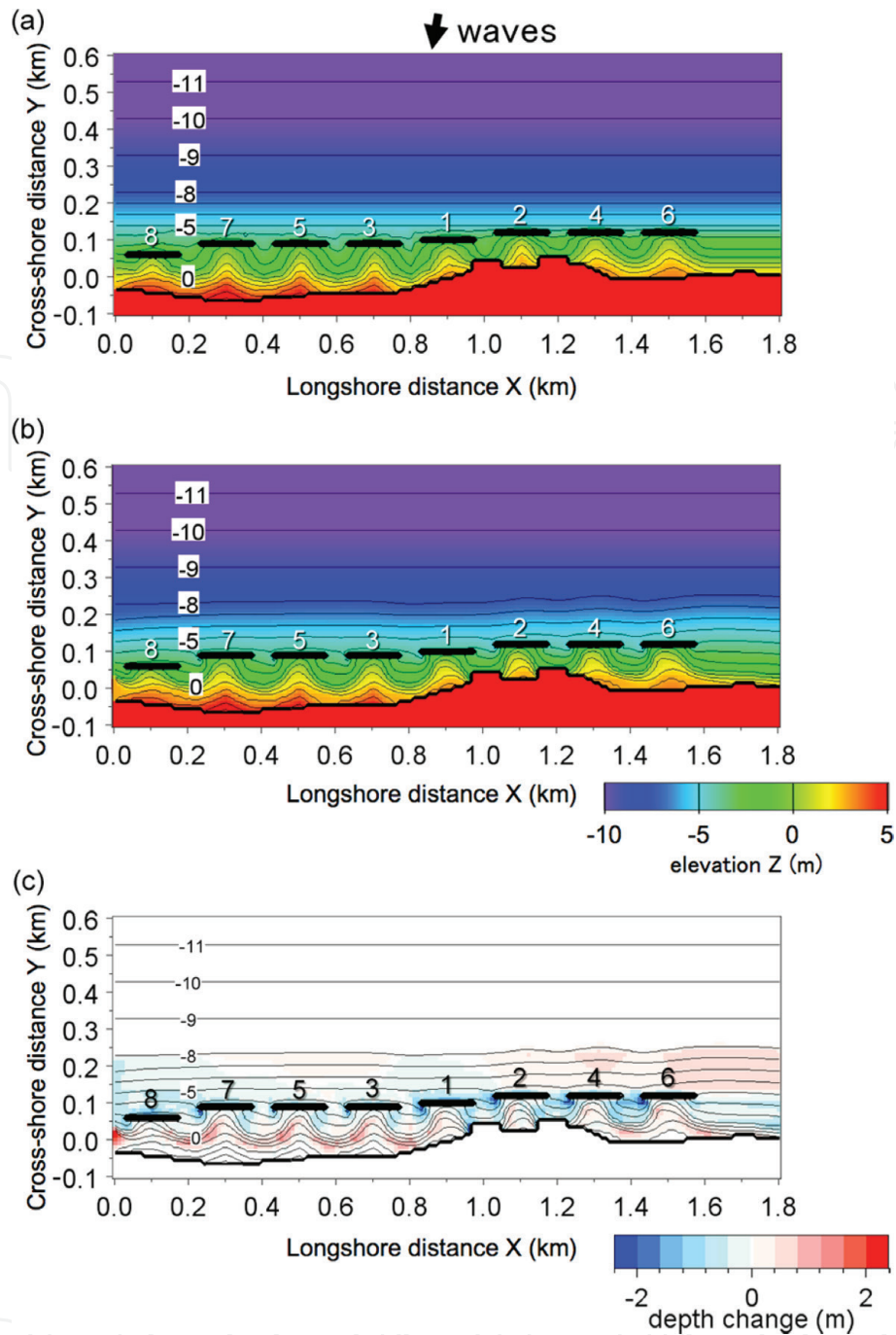


Figure 14. Predicted bathymetries after a 40-h wave action in case of detached breakwater [4] (a) Initial bathymetry, (b) After 40 hours (10^4 steps), (c) depth changes.

Figure 15(a) shows the initial bathymetry when the No. 3 detached breakwater was converted into an artificial reef. After a 40-h wave action, the tombolo rapidly disappeared, and tombolos with a symmetric shape at the initial stage became asymmetric while inclining leftward behind the No. 5 and No. 7 detached breakwaters west of the artificial reef (**Figure 15(b)**). Also, local scouring occurred at the west end of the artificial reef. The predicted results were in good agreement with the measured results, as shown in **Figure 13**. In the bathymetric changes (**Figure 15(c)**), the beach was eroded not only shoreward of the artificial reef but also near the area between the artificial reef and the No. 5 detached breakwater.

3.4.2 Change in wave field and nearshore currents

The wave field and nearshore currents were compared to investigate the difference between the topographic changes behind the detached breakwater and artificial reef

Calculation model	Type 8 BG model taking wave and nearshore current fields into account
Initial bathymetry	Bathymetry before the conversion of the detached breakwater into artificial reef Tomboles were set behind artificial reef Straight parallel contours with beach slope of 1/30 in offshore zone between -5 and -8 m and that of 1/100 in depth zone deeper than -8 m
Wave conditions	Incident waves: $H_I = 3$ m, $T = 8$ s, and wave direction $\theta_I = -10^\circ$ relative to normal to initial shoreline
Berm height	$h_R = 3$ m
Depth of closure	$h_c = 2.5H$ (H : wave height) The increment due to the effect of strong rip currents is evaluated as $h_c = \{1 + \alpha(v/u_m)\}h_c$ Here, V = velocity of nearshore currents, u_m = amplitude of seabed velocity due to orbital motion of waves, and $a = 0.5$ The lower and upper limits of h_c ' are 3 and 9 m, respectively
Equilibrium slope	$\tan\beta_c = 1/10$ shallower than -1 m $\tan\beta_c = 1/30$ between $Z = -1$ and -8 m $\tan\beta_c = 1/100$ deeper than -8 m
Angle of repose slope	$\tan\phi = 1/2$
Coefficients of sand transport	Coefficient of sand transport due to current $K_c = 7.5 \times 10^{-4}$ Coefficient of sand transport due to wave $K_w = 0.5K_c$
Mesh size	$\Delta x = \Delta y = 10$ m
Time intervals	$\Delta t = 0.004$ h
Duration of calculation	10^4 steps
Boundary conditions	Shoreward and landward ends $q_x = 0$ and right and left boundaries $dq_y/dy = 0$
Calculation of wave field	Energy balance Equation [6] <ul style="list-style-type: none"> • Term of wave dissipation due to wave breaking: Dally et al. [7] model • Mesh size: $\Delta x = \Delta y = 10$ m • Wave spectrum of incident waves: combination of frequency spectrum of Bretchnider-Mitsuyasu-type and Mitsuyasu-type directional function [8] • Total number of frequency components $N_F = 1$ and number of directional subdivisions $N_\theta = 8$ • Directional spreading parameter $S_{\max} = 10$ • Coefficient of wave breaking $K = 0.17$ and $\Gamma = 0.5$ • Minimum depth $h_{\min} = 1$ m • Imaginary depth between $Z = -h_0$ and berm height h_R: $h_0 = 3$ m • Wave energy = 0, where $Z \geq h_R$
Calculation of nearshore currents	• Two-dimensional shallow water momentum equation and continuity Equation [9] <ul style="list-style-type: none"> • Explicit finite difference method • Mesh size $\Delta x = \Delta y = 10$ m • Time intervals $\Delta t = 0.014$ s • Duration of calculation 5×10^4 steps • Friction coefficient $C_f = 0.01$ • Lateral diffusion coefficient $N = 0.5$ [10] • Minimum water depth $h_{\min} = 1$ m
Other remarks	• $\Gamma = 0.55$ on crown of artificial reef • Calculation of wave and nearshore currents: every 5000 steps of calculation of beach changes • Wave transmission coefficient of detached breakwater $K_t = 0.15$

Table 2.
Calculation conditions.

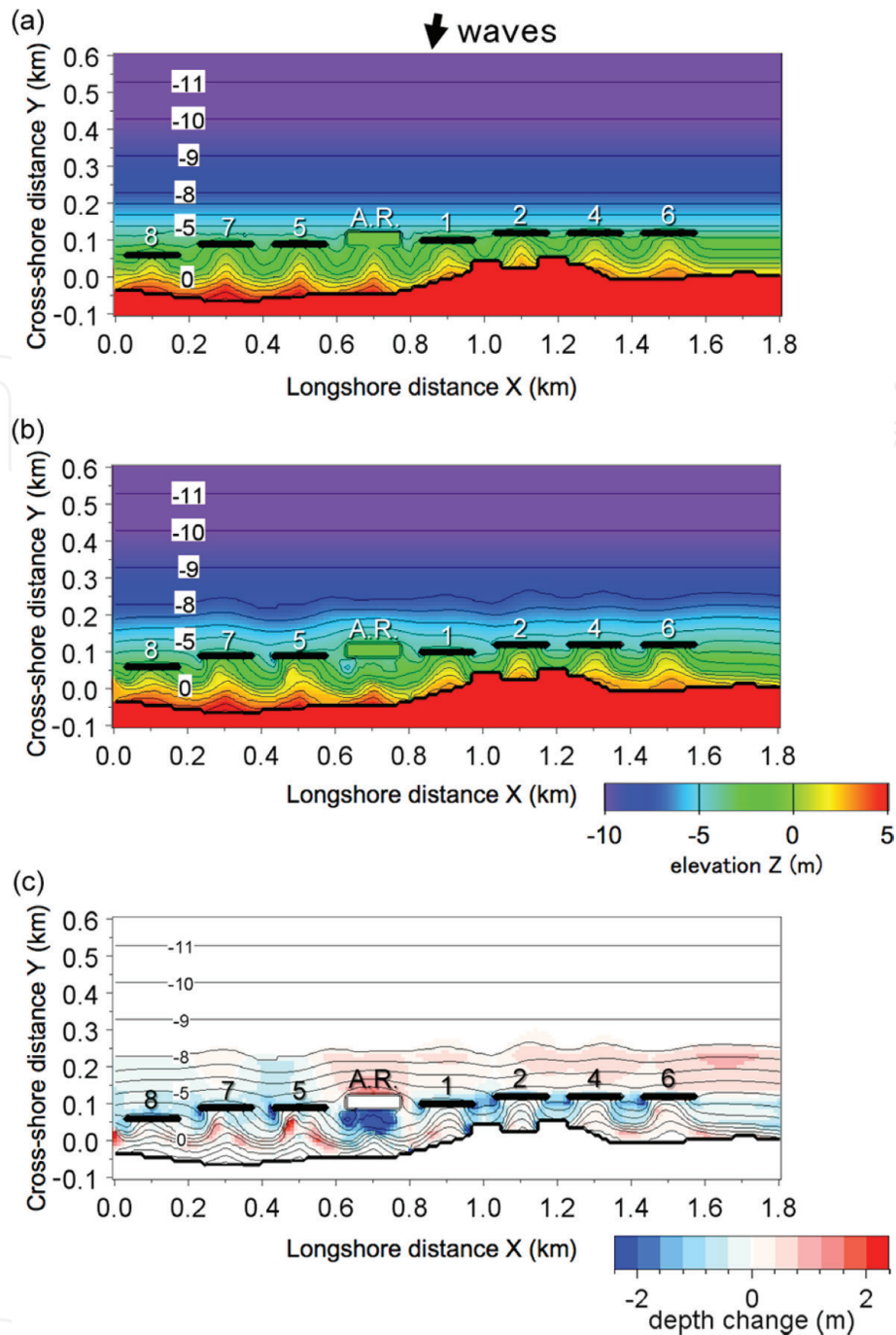


Figure 15. Predicted bathymetries after a 40-h wave action in case of artificial reef [4] (a) Initial bathymetry, (b) After 40 hours (10^4 steps), (c) depth changes.

(Figures 16 and 17). Although the wave height distributions around the detached breakwaters and artificial reef are similar, as shown in Figure 16(a) and 16(b), marked changes can be seen in the nearshore currents. In the case of the detached breakwater, a couple of circulating currents was generated on the lee of the detached breakwaters (Figure 17(a)), whereas strong shoreward currents were induced on the reef, and such currents reduced to rip currents obliquely flowing out at the opening between the artificial reef and the existing detached breakwater (Figure 17(b)). Because it was difficult for the seawater transported shoreward on the artificial reef to be carried offshore again only by the rip currents, part of the seawater passed through the lee of the detached breakwater and was finally returned to the offshore sea through the openings of the detached breakwaters. The generation of strong shoreward currents on the reef and oblique rip currents in the opening explains the difference between the topographic changes around the detached breakwaters and artificial reef.

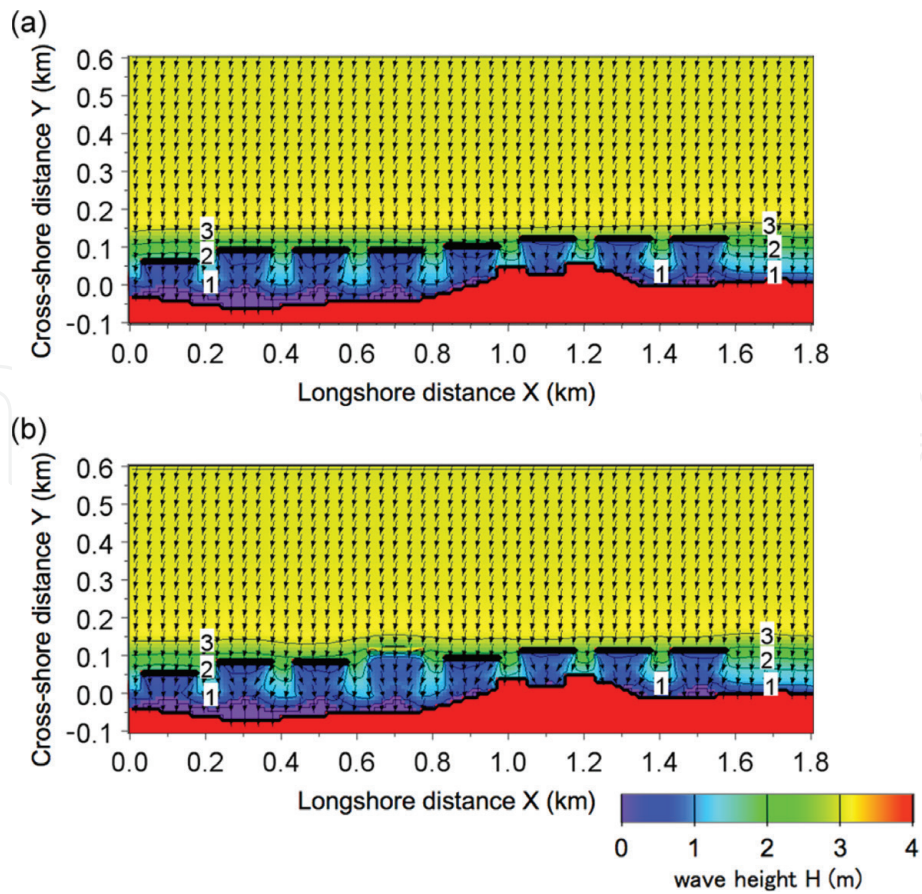


Figure 16. Wave fields around detached breakwater and artificial reef [4] (a) detached breakwater, (b) artificial reef.

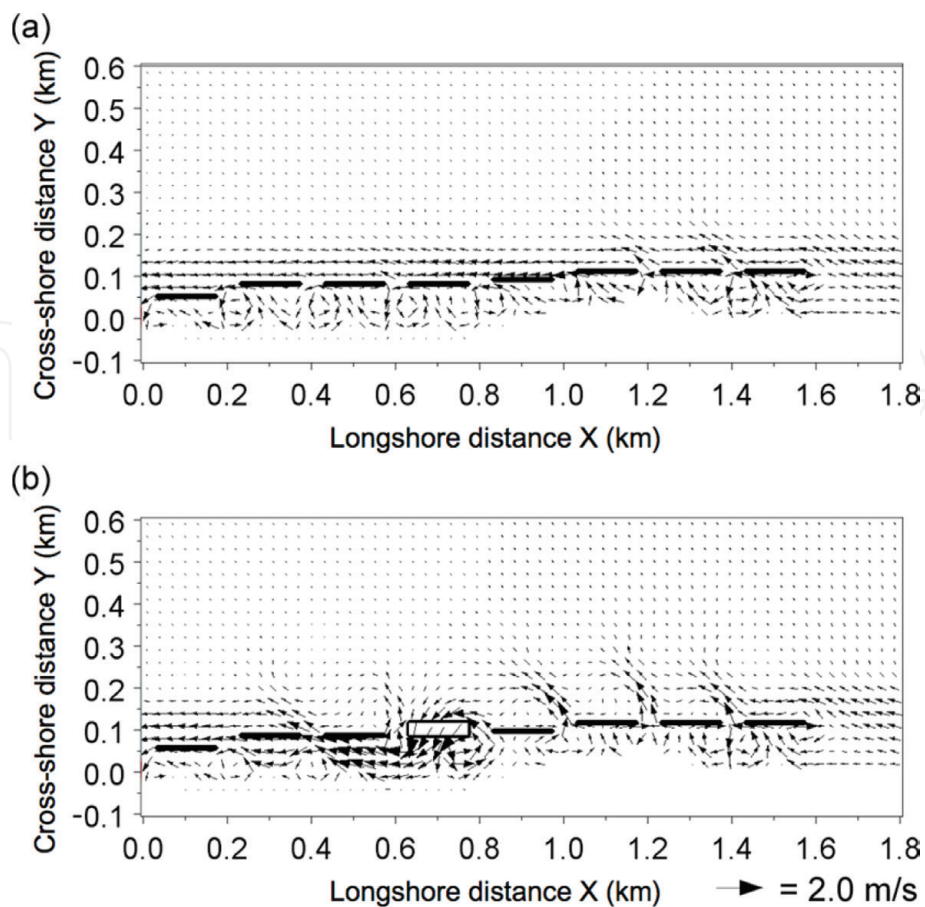


Figure 17. Nearshore currents around detached breakwater and artificial reef [4] (a) detached breakwater, (b) artificial reef.

4. Conclusions

In Chapter 4, two topics were discussed, and topographic changes were predicted, in which the effects by both waves and strong currents were taken into account:

(1) formation of dynamically stable ebb tidal delta (the Type 7 BG model) and (2) beach changes around artificial reef built on Kaike coast (the Type 8 BG model).

1. The development of an ebb tidal delta subject to the actions of waves and strong ebb tidal currents was investigated, taking Imagire-guchi inlet connecting Lake Hamana to the Pacific Ocean as an example. The predicted bathymetric changes were compared with the measured changes, and they were in good agreement.
2. The Type 8 BG model, in which the effect of the sand transport flux due to strong shoreward currents induced by wave breaking on the artificial reef was explicitly included, was used on the Kaike coast, where one of the detached breakwaters was converted into an artificial reef. After the storm, the tombolo behind the artificial reef was eroded, and a local scouring hole was formed in the opening. Given the storm wave conditions, beach changes were predicted. The beach changes were successfully predicted using this model.
3. It was concluded that shoreward currents on the artificial reef and resulted rip currents in the opening played an important role in the beach changes around the artificial reef and that the artificial reef was less effective in sand deposition effect than the detached breakwater.

Acknowledgements

Part of the work described in Chapter 4, i.e., prediction of formation of dynamically stable ebb tidal delta and beach changes around artificial reef built on Kaike coast, was based on the conference paper [3, 4] presented at the 32nd and 33rd Conference on Coastal Engineering in 2010 and 2012, respectively. We would like to express our gratitude for the use of materials.

IntechOpen

IntechOpen

Author details


Takaaki Uda^{1*}, Masumi Serizawa² and Shiho Miyahara²

1 Public Works Research Center, Tokyo, Japan

2 Coastal Engineering Laboratory Co., Ltd., Tokyo, Japan

*Address all correspondence to: uda@pwrc.or.jp

IntechOpen

© 2018 The Author(s). Licensee IntechOpen. Distributed under the terms of the Creative Commons Attribution - NonCommercial 4.0 License (<https://creativecommons.org/licenses/by-nc/4.0/>), which permits use, distribution and reproduction for non-commercial purposes, provided the original is properly cited. 

References

- [1] Syamsidik, Aoki S, Kato S. Effects of tidal currents and waves on bottom suspended sediment fluxes off two river mouths. Proceedings of 18th International Offshore (Ocean) and Polar Engineering Conference. Vancouver; 2008
- [2] Serizawa M, Uda T, San-nami T, Furuike K, Ishikawa T. Model for predicting formation of dynamically stable ebb tidal delta off tidal inlet. In: Proceedings of 31st ICCE. 2008. pp. 2291-2302
- [3] Uda T, Serizawa M, San-nami T, Ishikawa T. Prediction of formation of dynamically stable ebb tidal delta and measures for preventing offshore sand loss. In: Proceedings of 32nd ICCE, sediment. 73. 2010. pp. 1-10 https://icce-ojs-tamu.tdl.org/icce/index.php/icce/article/view/1047/pdf_163
- [4] Fujiwara H, Uda T, Onishi T, Miyahara S, Serizawa M. Prediction of beach changes around artificial reef using BG model. In: Proceedings of 33rd ICCE, sediment. 77. 2012. pp. 1-12 https://icce-ojs-tamu.tdl.org/icce/index.php/icce/article/view/6532/pdf_533
- [5] Uda T. Japan's Beach Erosion: Reality and Future Measures. 2nd ed. Singapore: World Scientific; 2017. 530 p
- [6] Mase H. Multidirectional random wave transformation model based on energy balance equation. Coastal Engineering Journal, JSCE. 2001;43(4):317-337
- [7] Dally WR, Dean RG, Dalrymple RA. A model for breaker decay on beaches. In: Proceedings of 19th ICCE. 1984. pp. 82-97 <https://journals.tdl.org/icce/index.php/icce/article/view/3787/3470>
- [8] Goda Y. Random Seas and Design of Maritime Structures. Tokyo: University of Tokyo Press; 1985. 323 p
- [9] Horikawa K. Nearshore Dynamics and Coastal Processes. Tokyo: University of Tokyo Press; 1988. 522 p
- [10] Larson M, Kraus NC. Numerical model of longshore current for bar and trough beaches. Journal of Waterway, Port, Coastal, and Ocean Engineering. 1991;117(4):326-347